Supporting information for

Environmental significance of kaolinite variability over the last centuries in crater lake sediments from Central Mexico

Nathalie Fagel[1], Isabel Israde-Alcantara[2], Reza Safaierad[1], Marttiina Rantala[1], Sabine Schmidt[3], Gilles Lepoint[4], Pierre Pellenard[5], Nadine Mattielli[6] and Sarah Metcalfe[7]

1. AGEs, Department of Geology, Université de Liège, Belgium, nathalie.fagel@uliege.be.
2. Instituto de Investigaciones en Ciencias de la Tierra, Universidad Michoacana de San Nicolás de Hidalgo. Morelia, Michoacán, México
3. Univ. Bordeaux, CNRS, Bordeaux INP, EPOC, UMR 5805, F-33600 Pessac, France
4. LETIS, Université de Liège, Belgium
5. Biogéosciences UMR 6282 CNRS/ub/EPHE, University of Burgundy, Dijon, France
6.G-Time, Université Libre de Bruxelles, Belgium
7. School of Geography, University of Nottingham, Nottingham NG7 2RD, United Kingdom

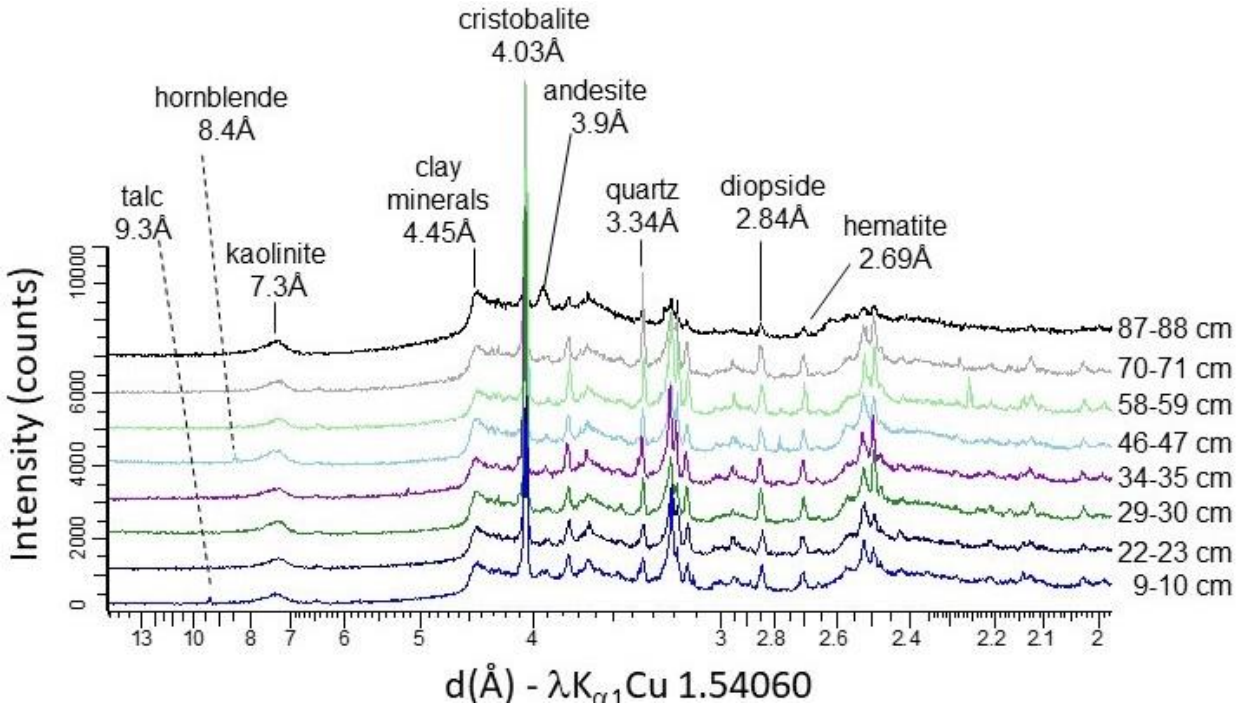

Figure S1. Comparison of XRD spectra measured on bulk sediment powders of core LTa19-3 with identification of the main minerals. The reflection at 4.45Å corresponds to the common reflection of clay minerals, represented here by kaolinite.

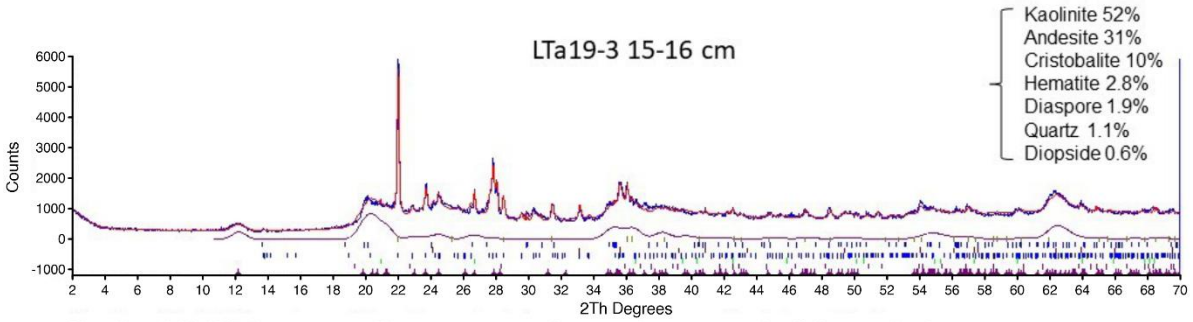

Figure S2. Example of Topas-derived reconstructed profile (red curve) with the raw XRD profile (blue curve) for the sample LTa19-3 15-16 cm. The quantification of the different identified mineral phases is given on the right side of the figure.

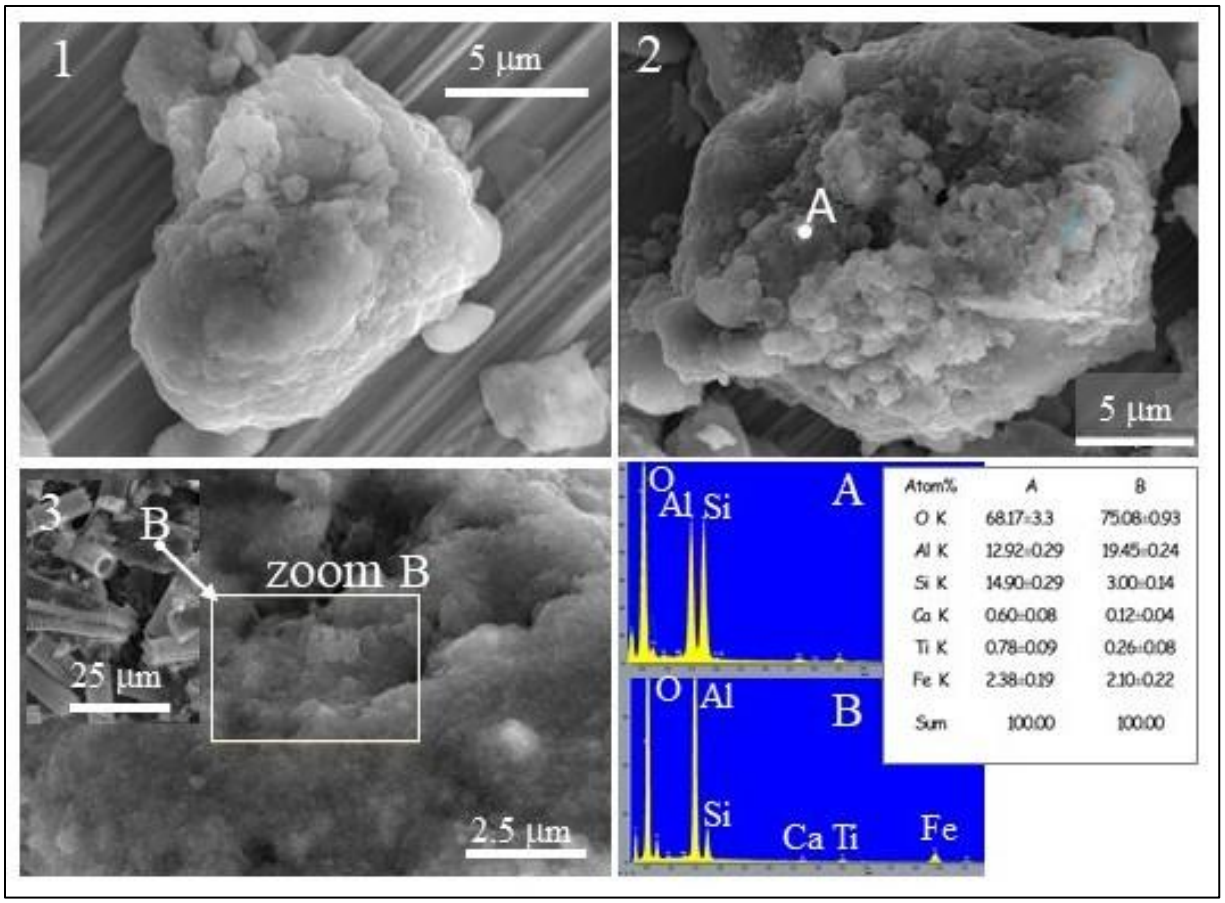

Figure S3. SEM images of kaolinite particles from sample LLEs19-2 45-46 cm (photo 1 and 2) with EDX composition of particle A located in photo 2; SEM image (photo 3) from sample LTa19-3 51-52 cm and EDX composition of crystal B located in photo 3B. The EDX composition of areas A and B are given as atomic %. The composition of A corresponds to a kaolinitic particle whereas the composition of B is consistent with diaspore. The SEM-EDX observations have been made at the University of Bourgogne (Dijon, France).

(a). LLEs19-2

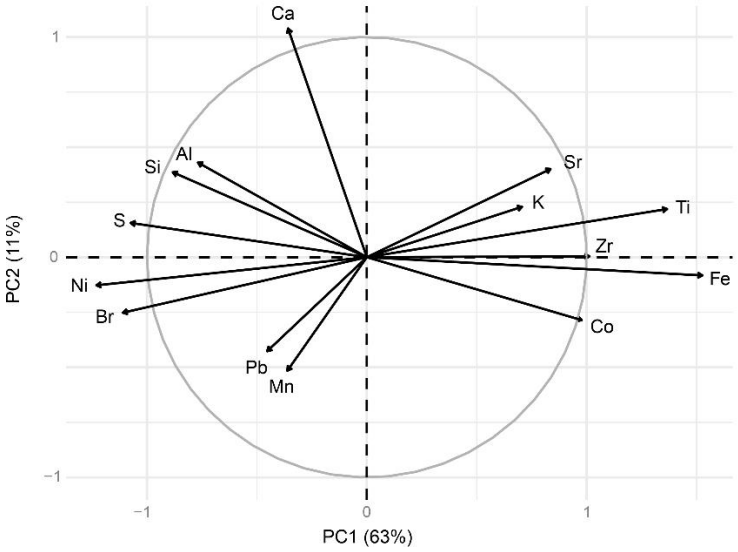

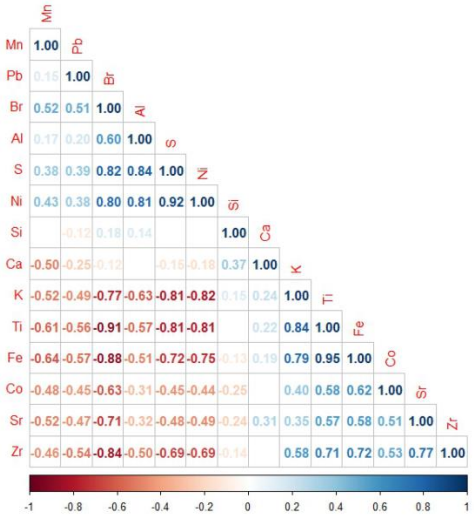

(b). LTa19-3

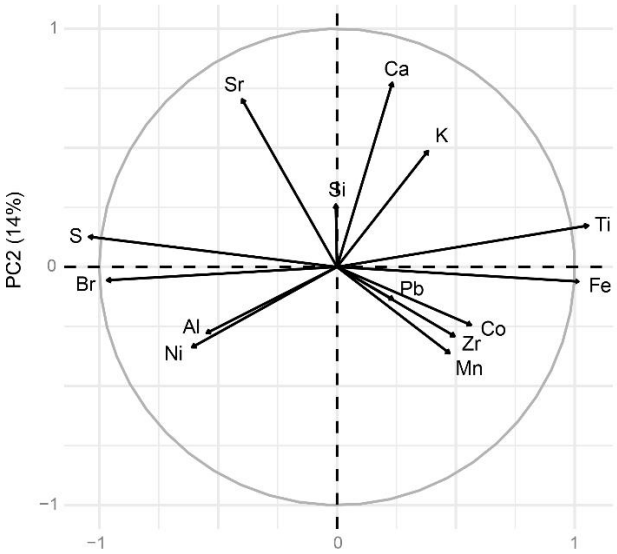

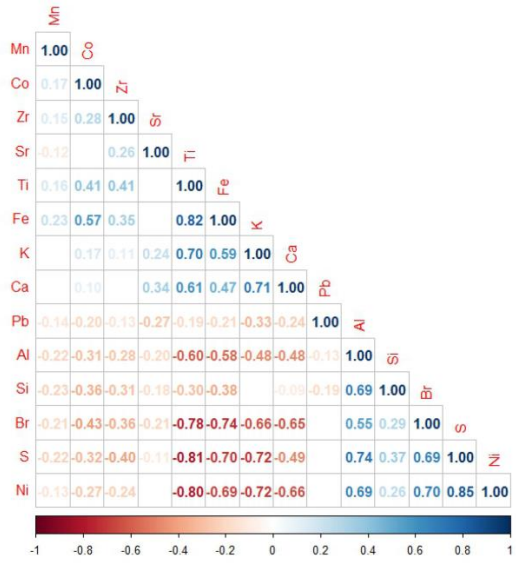

(c). LTe19-4

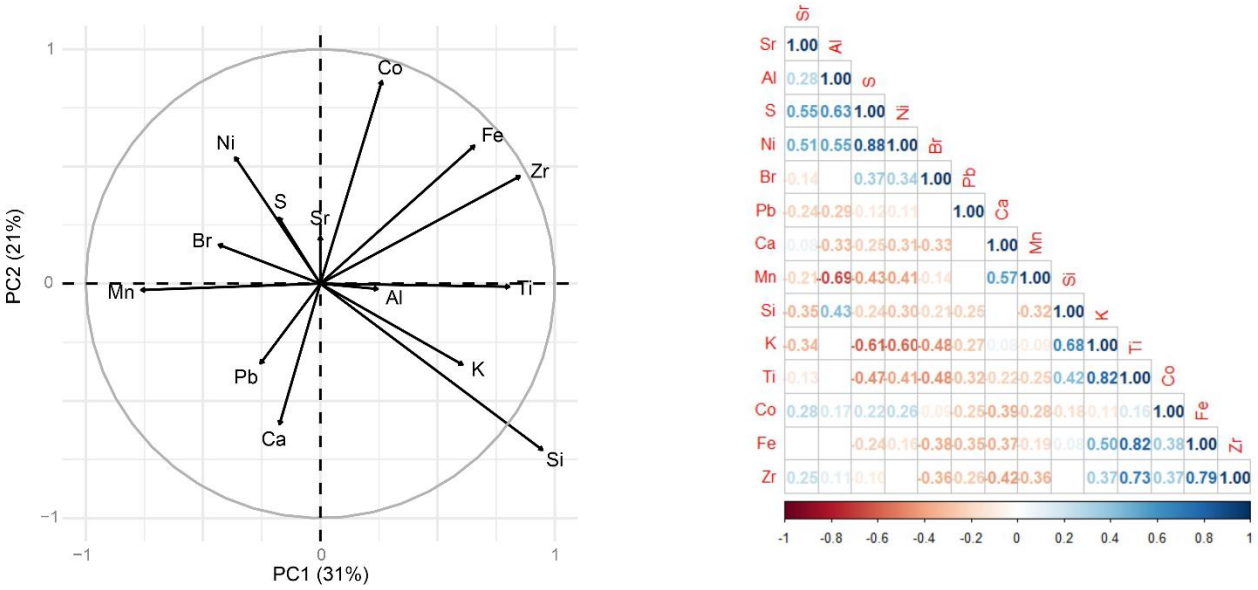

Figure S4. PC1-PC2 biplot diagram established from the X-ray fluorescence (XRF) core scanner and correlation coefficient matrix of XRF core scanner data (14 elements) for the three lacustrine cores LLEs19-2 (a), LTa19-3 (b) and LTe19-4 (c). The lower scale gives the strength of the correlation (negative in red, positive in blue). Only significant correlations (p value < 0.01) are displayed in the matrix.

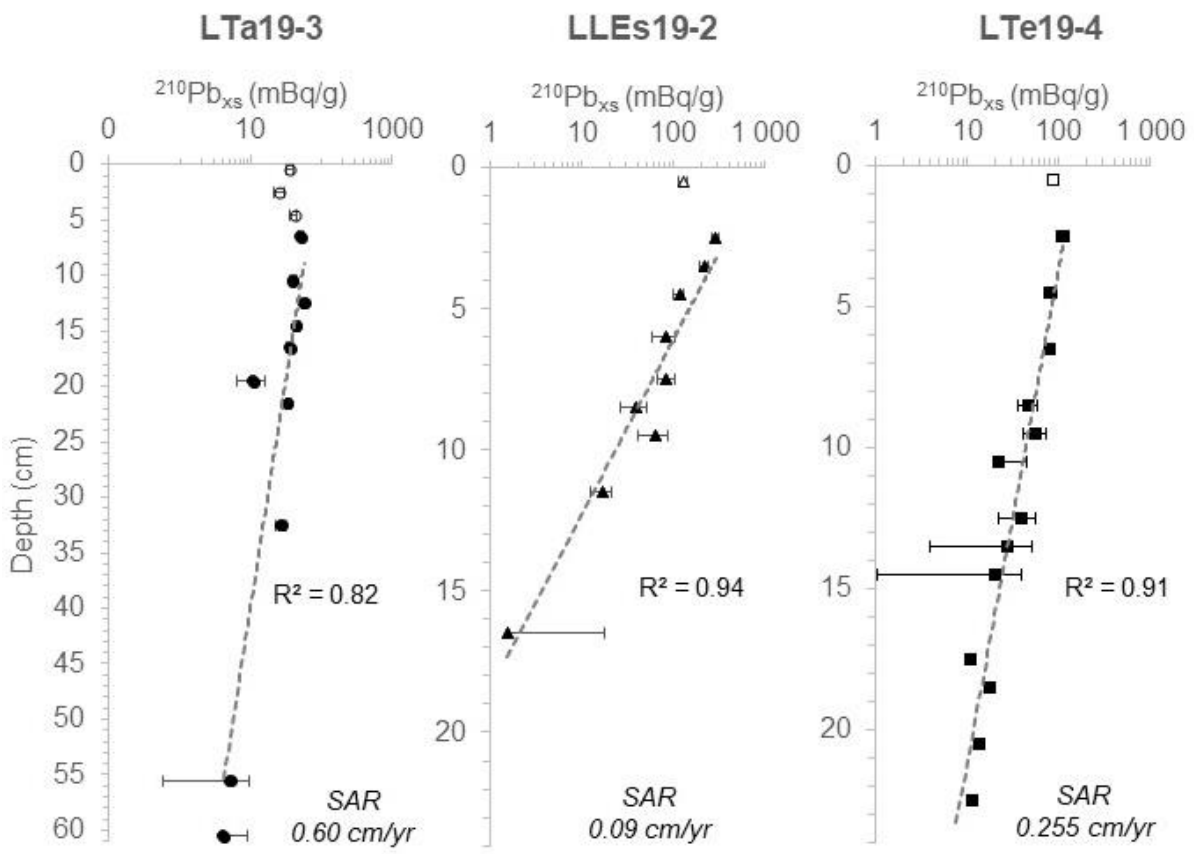

Figure S5. ^{210}Pbxs profiles in the upper part of cores LLEs19-2 (0-17 cm), LTa19-3 (0-61 cm) and LTe19-4 (0-23 cm). The dark symbols show the levels used to estimate sediment accumulation rate (SAR).

(a)

STe22-3 XRD on bulk powder

Kaolinite unit cell parameters modified from Bish D.L. (1993) Rietveld Refinement of the Kaolinite Structure at 1.5 K. Clays and clay minerals, 41(6), 738–744 https://doi.org/10.1346/CCMN.1993.0410613

kaolinite unit cell parameters

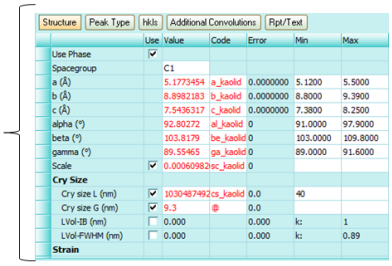

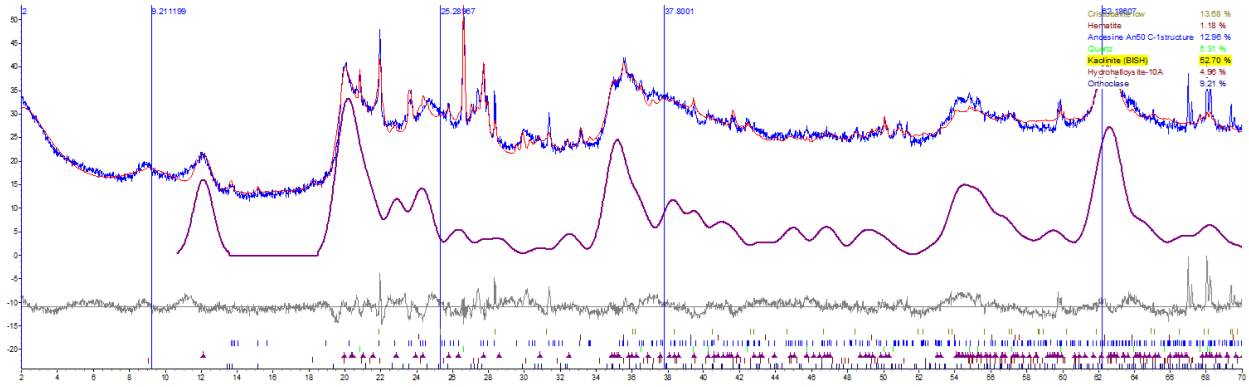

(b)

STe22-3 XRD on bulk powder

Kaolinite unit cell parameters modified from Bish D.L. (1993) Rietveld Refinement of the Kaolinite Structure at 1.5 K. Clays and clay minerals, 41(6), 738–744 https://doi.org/10.1346/CCMN.1993.0410613

Hydrohalloysite unit cell parameters

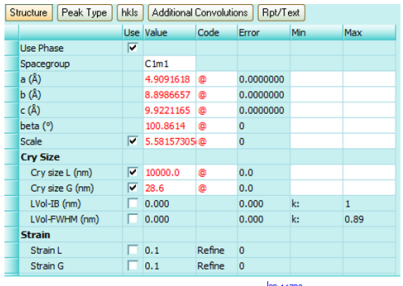

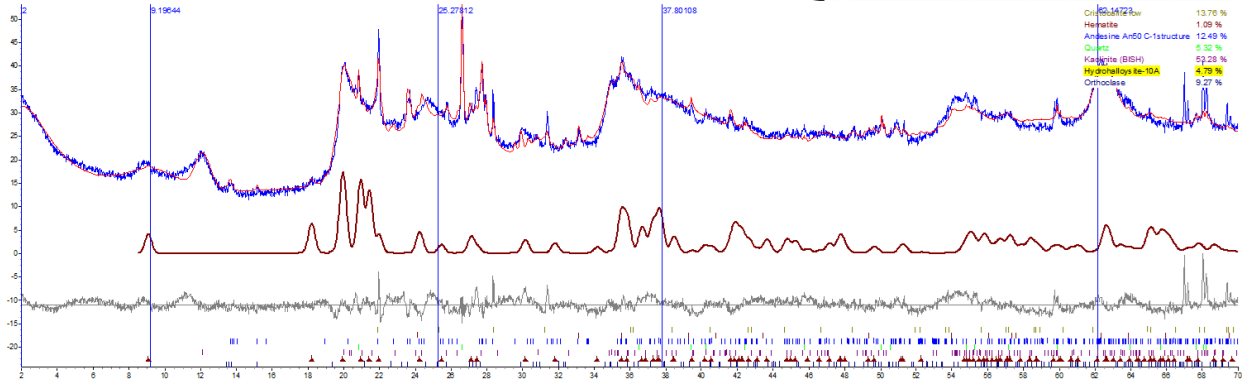

Figure S6. Comparison between reconstructed XRD pattern (red curve) and raw pattern (blue curve) for soil sample STe22-3 from Lake Teremendo (19°48'22.8"N, 101°27'4.9"W). Reconstructed contribution (brown curve) and unit cell parameters reported for kaolinite (a) and hydrohalloysite (b). The calculated abundance of the mineral phases is given on the left side of the XRD spectra.

Table S1a. Grain-size distribution of samples from core LLEs19-2.

Core LLEs19-2												
Sample	Mid-depth (cm)	clay % < 2 µm	silt % 2-63 µm	sand % > 63 µm	fine % ≤10 µm	silt 2-63 µm %			sand > 63 µm %			
						2-10	10-30	30-63	63-125	125-250	250-500	500-1000
2-3	2.75	1.41	69.0	29.5	14.3	12.9	26.8	29.3	18.5	8.21	0.95	0.0
7.5-8	7.75	2.09	72.8	25.1	19.5	17.5	29.5	25.9	15.1	8.05	1.70	0.0
10-11	10.5	2.71	76.0	21.3	19.6	16.9	33.6	25.4	14.9	5.54	0.81	0.0
14-15	14.5	4.32	66.8	28.8	20.9	16.6	25.5	24.7	18.9	9.26	0.64	0.0
17-17.5	17.25	2.39	78.3	19.3	19.1	16.7	39.2	22.4	12.6	4.06	2.20	0.40
18-19	18.5	1.78	71.6	26.7	14.5	12.8	34.3	24.5	12.4	9.52	4.76	0.0
21-22	21.5	1.30	79.0	19.7	14.6	13.3	39.7	25.9	14.3	4.92	0.53	0.0
23-24	23.5	1.42	82.4	16.2	17.8	16.3	40.6	25.4	12.2	3.82	0.19	0.0
29-30	29.5	1.69	86.6	11.7	21.6	19.9	44.2	22.5	8.28	2.83	0.57	0.0
34-35	34.5	3.98	71.9	24.1	23.7	19.6	30.8	21.4	15.9	7.28	0.88	0.0
36-37	36.5	3.32	79.8	16.9	24.6	21.2	36.9	21.5	12.0	4.04	0.77	0.0
40-41	40.5	3.22	79.9	16.9	26.1	22.9	38.3	18.7	11.4	4.26	1.22	0.0
45-46	45.5	2.93	79.3	17.8	23.5	20.6	37.7	20.9	12.7	3.96	1.07	0.04
48-49	48.5	2.83	81.4	15.7	23.9	21.1	39.8	20.5	11.6	3.48	0.60	0.0
52-52.5	52.25	2.60	79.8	17.5	21.7	19.1	39.6	21.0	11.7	5.06	0.77	0.0
mean		2.61	77.5	19.8	20.8	18.2	36.4	22.9	13.1	5.43	1.19	0.03
std		0.91	5.18	4.80	3.53	2.98	5.07	2.35	2.54	2.19	1.15	0.12
min		1.30	66.8	11.7	14.5	12.8	25.5	18.7	8.28	2.83	0.19	0.0
max		4.32	86.6	29.5	26.1	22.9	44.2	25.9	18.9	9.52	4.76	0.43

Table S1b. Grain-size distribution of samples from core LTa19-3.

Core LTa19-3												
Sample	Mid-depth (cm)	clay % < 2 µm	silt % 2-63 µm	sand % > 63 µm	fine % ≤10 µm	silt 2-63 µm %			sand > 63 µm %			
						2-10	10-30	30-63	63-125	125-250	250-500	500-1000
0-1	0.5	4.20	83.2	16.8	28.0	23.8	34.6	205	11.8	2.75	1.60	0.68
4-5	4.5	5.34	78.6	21.4	28.1	22.7	32.8	17.7	10.9	8.52	2.00	0.0
9-10	9.5	6.11	90.3	9.74	36.2	30.1	35.8	18.3	7.23	1.27	1.06	0.18
13-14	13.5	3.88	79.7	20.3	24.2	20.3	33.4	22.1	12.0	4.47	3.12	0.71
17-18	17.5	4.25	77.5	22.5	27.3	23.0	32.5	17.8	9.69	5.49	5.73	1.55
22-23	22.5	4.34	76.3	23.7	25.5	21.1	31.7	19.1	10.4	4.28	6.27	2.75
26-27	26.5	5.76	76.3	23.7	32.3	26.5	27.9	16.1	10.2	6.57	4.99	1.94
30-31	30.5	5.31	81.2	18.8	29.3	24.0	32.1	19.8	8.87	3.75	4.69	1.48
35-36	35.5	5.88	80.7	19.3	34.5	28.6	29.5	16.7	11.7	6.05	1.30	0.22
39-40	39.5	14.8	92.8	7.17	57.9	43.2	26.3	8.54	3.23	1.32	2.05	0.57
43-44	43.5	10.3	78.6	21.3	45.5	35.2	23.9	9.20	5.28	1.62	10.2	4.28
47-48	47.5	10.3	90.0	9.96	48.7	38.4	28.8	12.5	4.68	0.80	3.03	1.45
51-52	51.5	12.8	98.4	1.63	58.1	45.2	31.2	9.11	1.64	0.0	0.0	0.0
55-56	55.5	4.00	70.5	29.5	24.4	20.4	26.6	19.5	15.4	9.53	4.07	0.52
59-60	59.5	4.04	66.3	33.7	22.2	18.2	25.3	18.8	15.2	9.58	6.96	1.97
63-64	63.5	3.85	74.2	25.8	26.6	22.8	28.9	18.6	13.5	6.52	4.07	1.72
67-68	67.5	3.00	80.0	20.1	23.5	20.5	33.2	23.3	13.3	4.03	2.20	0.49
71-72	71.5	2.20	75.1	24.9	19.3	17.1	31.4	24.4	15.0	5.85	3.31	0.63
75-76	75.5	2.65	77.5	22.5	21.9	19.3	32.0	23.6	14.7	5.32	2.09	0.41
79-80	79.5	2.84	81.3	18.7	24.5	21.7	33.2	23.5	13.2	3.61	1.46	0.44
84-85	84.5	3.75	78.8	21.2	24.7	21.0	32.2	21.9	13.3	4.55	2.4	0.92
88-89	88.5	2.56	77.6	22.4	25.2	22.6	32.4	20.1	13.4	5.07	2.77	1.13
mean		5.55	80.2	19.8	31.3	25.7	30.7	18.2	10.7	4.59	3.43	1.09
std		3.48	7.40	7.40	11.5	8.12	3.07	4.78	4.09	2.70	2.35	1.04
min	-	2.20	66.3	1.64	19.3	17.1	23.9	8.54	1.64	0.0	0.0	0.0
max		14.8	98.4	33.7	58.1	45.2	35.8	24.4	15.4	9.58	10.2	4.28

Table S1c. Grain-size distribution of samples from core LTe19-4.

Core LTe19-4												
Sample	Mid-depth (cm)	clay % < 2 µm	silt % 2-63 µm	sand % > 63 µm	fine % ≤10 µm	silt 2-63 µm %			sand > 63 µm %			
						2-10	10-30	30-63	63-125	125-250	250-500	500-1000
0-1	0.5	1.53	70.9	27.5	9.30	7.80	37.3	25.9	19.7	5.06	2.05	0.65
5-6	5.5	2.50	74.2	23.2	13.0	10.5	35.3	28.4	19.4	3.80	0.0	0.0
10-11	10.5	2.98	74.3	22.8	16.7	13.7	36.4	24.2	16.7	3.64	1.71	0.57
15-16	15.5	2.46	71.2	26.4	13.0	10.5	31.2	29.4	19.1	4.97	1.76	0.58
20-21	20.5	2.59	75.2	22.2	14.0	11.4	34.4	29.4	17.0	3.63	1.19	0.41
24-25	24.5	4.03	80.5	15.5	20.8	16.8	41.3	22.4	13.5	1.99	0.0	0.0
35-36	35.5	3.54	79.7	16.7	17.9	14.4	39.9	25.4	14.4	2.38	0.0	0.0
40-41	40.5	4.41	80.6	15.0	23.0	18.6	42.6	19.3	13.0	2.01	0.0	0.0
45-46	45.5	5.30	81.0	13.7	27.6	22.3	41.3	17.4	11.6	2.06	0.0	0.0
50-51	50.5	3.74	76.8	19.4	17.4	13.6	35.2	27.9	17.4	2.04	0.0	0.0
55-56	55.5	4.14	80.3	15.5	20.8	16.7	37.5	26.1	14.1	1.40	0.0	0.0
61-62	61.5	4.39	81.6	14.0	22.6	18.2	38.5	24.9	12.5	1.50	0.0	0.0
65-66	65.5	4.13	71.5	24.4	19.1	15.0	31.8	24.7	16.5	3.48	3.05	1.30
70-71	70.5	2.74	60.1	37.1	13.7	11.0	28.4	20.7	14.9	1.90	1.00	4.12
75-76	75.5	3.54	79.7	16.8	18.9	15.4	42.0	22.3	14.6	2.18	0.0	0.0
80-81	80.5	3.32	75.0	21.7	18.1	14.8	36.2	24.0	13.8	2.95	3.72	1.16
85-86	85.5	3.30	74.4	22.2	16.5	13.2	36.2	25.0	15.4	3.52	2.78	0.48
90-91	90.5	3.44	68.3	27.9	17.7	14.2	32.0	22.3	15.1	7.27	4.74	0.84
94-95	94.5	3.98	74.4	21.6	19.4	15.5	36.7	22.2	14.9	3.98	2.13	0.55
100-101	100.5	1.33	54.1	44.6	8.14	6.80	24.6	22.7	20.7	11.5	8.82	3.50
104-105	104.5	2.79	65.4	31.8	12.6	9.78	34.2	21.5	20.2	5.53	4.50	1.59
109-110	109.5	4.96	72.8	22.2	21.7	16.7	34.0	21.1	15.5	4.23	1.91	0.62
mean		3.42	73.8	22.8	17.4	13.9	35.8	24.0	15.9	3.68	1.79	0.74
std		1.00	6.98	7.68	4.65	3.69	4.44	3.16	2.60	2.28	2.20	1.10
min		1.33	54.1	13.7	8.14	6.80	24.6	17.4	11.6	1.40	0.0	0.0
max		5.29	81.6	44.6	27.6	22.3	42.7	29.4	20.8	11.5	8.82	4.12

Table S2a. Mineralogical data for core LLEs19-2 derived from X-ray diffraction (XRD) on bulk sediment powder. In the table, each mineral is represented by its relative ponderal abundance (in %) using Eva ® Bruker software.

Core LLEs19-2											
Depth (cm)	Andesite	Kaolinite	Diopside	Hornblende	Forsterite	Quartz	Cristobalite	Calcite	Aragonite	Dolomite	Talc
3-4	39	36	6.9		2.7	2.0	1.2	6.8	4.7	0	0.3
7.5-8	39	38	9.6		2.5	1.1	3.0	3.1	4.4	0	0
14-15	59	22	12		5.6	1.6	0.5	0	0	0	1.0
18-19	27	43	3.9			1.6	3.7	15	5.4	0	0
23-24	26	45	4.4	1.0		1.1	4.1	12	5.4	2.1	0
35-36	54	27	7.4			1.0	0.6	5.1	5.1	0	0
35-40	55	30	7.1			1.2	0.6	3.1	0.0	0	0
40-41	55	21	5.5	1.9		3.3	2.1	5.4	6.0	0	0
45-46	35	27	7.3			1.6	9.9	9.0	8.9	0	0
50-51	39	36	5.9			1.6	3.5	5.9	6.6	1.8	0
mean	43	33	7.0	1.4	3.6	1.6	2.9	6.6	4.6	0.4	0.1
std	12	8.3	2.3	0.6	1.8	0.7	2.8	4.5	2.8	0.8	0.3
min	26	21	3.9	1.0	2.5	1.0	0.5	0	0	0	0
max	59	45	12	1.9	5.6	3.3	9.9	15	8.9	2.1	1.0

Table S2b. Mineralogical data for core LTa19-3 derived from X-ray diffraction (XRD) on bulk sediment powder. In the table, each mineral is represented by its relative ponderal abundance (in %) using Eva ® Bruker software. The reported results correspond to an average of 5 analyses made on a 1 cm-thick slice of sediments.

Core LTa19-3											
Depth (cm)	Andesite	Kaolinite	Diaspore	Diopside	Hornblende	Forsterite	Quartz	Cristobalite	Hematite	Magnetite	Talc
0-5	29	48	1.6	0.58	0.91		1.9	13	2.9	1.9	
5-10	29	54	1.6	0.56	0.46		1.5	9.8	2.5	1.3	0.7
10-15	30	51	1.8	0.57	0.39		1.6	11	3.1	1.4	
15-20	31	51	1.9	0.62			1.4	11	2.9		
20-24	29	51	1.5	0.54	0.64		1.7	13	3.1		
25-30	21	64	0.92	0.35	1.7		1.2	8.1	2.2		
30-35	22	65	1.5	0.28	0.81		1.7	6.7	1.7		
35-40	21	67	1.6	0.37			1.2	6.0	2.0	2.1	
40-45	24	64	1.5	0.43			1.7	6.6	1.8	1.9	
46-51	21	63	1.4	0.38	2.03	1.60	1.4	6.9	1.9	2.1	
51-55	24	63	1.3	0.43	1.5		2.0	6.5	1.6		
55-60	27	48	1.3	0.30	2.70		2.4	16	2.6		
60-65	19	57	4.9	0.13	0.45		2.5	12	3.7		
66-71	22	54	5.7	0.30	0.00		1.8	13	2.8	1.2	
71-75	27	48	4.2	0.42	1.5		2.1	13	2.7	1.6	
75-80	26	49	5.5	0.34	1.6		1.4	13	2.5	0.92	
81-85	24	53	4.2	0.17	1.4		1.2	14	2.5	0.62	
85-90	10	74	6.3	0.03	2.3		0.36	5.2	1.0	0.42	
90-92	16	70	3.3	0.15	2.3		0.88	6.2	1.4		
mean	24	58	2.7	0.36	1.3		1.6	10	2.4	1.4	
std	5	8.4	1.8	0.17	0.79		0.51	3.3	0.68	0.57	
min	10	48	0.92	0.03	0.00	1.60	0.36	5.2	1.0	0.42	0.66
max	31	74	6.3	0.62	2.7	1.60	2.5	16	3.7	2.1	0.66

Table S2c. Mineralogical data for core LTe19-4 derived from X-ray diffraction (XRD) on bulk sediment powder. In the table, each mineral is represented by its relative ponderal abundance (in %) using Eva ® Bruker software.

Core LTe19-4											
Depth (cm)	Andesite	Kaolinite	Diopside	Hornblende	Forsterite	Quartz	Cristobalite	Hematite	Calcite	Dolomite	Pyrite
0-1	39	51	6.8			2.4	1.3				
10-11	35	48	7.4			3.3	2.1		4.5		
15-16	43	48				3.0			6.1		
20-21	40	41			5.7	3.5			7.2	2.6	
24-25	40	46				2.3			9.4	2.5	
30-31	37	51				3.4			5.5	2.6	
35-36	39	52				2.7			4.2	2.4	
40-41	37	53				3.1			4.0	2.3	
45-46	37	54				3.4		1.6	2.5	2.4	
50-51	40	50				3.7		1.6	3.1	2.2	
54-55	43	41		0.3	6.3	3.9		1.0	2.4	2.2	
61-62	36	54				2.6		1.7	5.4		
65-66	39	52				3.0		1.4	2.4	2.5	
70-71	35	55				2.5		1.5	3.0	2.3	
75-76	35	59				1.9		1.6	3.0		
80-81	36	57				1.7		1.7	2.8		
85-86	35	59				1.9		1.8	2.4		
90-91	37	55				3.0		0.9	2.2		1.3
94-95	36	58				2.1		1.1	2.3		0.6
100-101	28	65				1.1		0.9	2.3	2.4	
104-105	42	48				3.0		1.2	2.0	2.6	
109-110	46	46				2.1		1.7	1.8	2.4	
mean	38	52	7.1		6.0	2.7	1.7	1.4	3.7	2.4	
std	3.7	5.9	0.5		0.4	0.7	0.5	0.3	2.0	0.2	
min	28	41	6.8	0.3	5.7	1.1	1.3	0.90	1.8	2.2	
max	46	65	7.4	0.3	6.3	3.9	2.1	1.8	9.4	2.6	

Text S1. Cif files obtained for kaolinite (a) and hydrohalloysite (b) after Rietveld refinement on a surface soil sample of the crater lake Teremendo, STe22-3 (19°48’22.8”N, 101°27’4.9”W).

(a) Kaolinite

```
data_
_chemical_name_mineral ?Kaolinite (BISH)?
_cell_length_a  5.177345
_cell_length_b  8.898218
_cell_length_c  7.543632
_cell_angle_alpha 92.80272
_cell_angle_beta  103.8179
_cell_angle_gamma 89.55465
_cell_volume 337.0647
_symmetry_space_group_name_H-M C1
loop_
_symmetry_equiv_pos_as_xyz
        'x, y, z'
        'x+1/2, y+1/2, z'
loop_
_atom_site_label
_atom_site_type_symbol
_atom_site_symmetry_multiplicity
_atom_site_fract_x
_atom_site_fract_y
_atom_site_fract_z
_atom_site_occupancy
_atom_site_B_iso_or_equiv
s1 SI+4   2 0.9942 0.3393 0.0909 1 0.44
s2 SI+4   2 0.5064 0.1665 0.0913 1 0.44
s3 AL+3   2 0.2971 0.4957 0.4721 1 0.83
s4 AL+3   2 0.7926 0.33 0.4699 1 0.83
s5 O-2   2 0.0501 0.3539 0.317 1 0.71
s6 O-2   2 0.1214 0.6604 0.3175 1 0.71
s7 O-2   2 0 0.5 0 1 0.71
s8 O-2   2 0.2085 0.2305 0.0247 1 0.71
s9 O-2   2 0.2012 0.7657 0.0032 1 0.71
s10 O-2   2 0.051 0.9698 0.322 1 0.9
s11 O-2   2 0.9649 0.1665 0.6051 1 0.9
s12 O-2   2 0.0348 0.4769 0.608 1 0.9
s13 O-2   2 0.0334 0.857 0.6094 1 0.9
```

(b) Hydrohalloysite

```
data_
_chemical_name_mineral ?Hydrohalloysite-10A?
_cell_length_a  4.909162
_cell_length_b  8.898666
_cell_length_c  9.922116
_cell_angle_alpha 90
_cell_angle_beta  100.8614
_cell_angle_gamma 90
_cell_volume 425.6827
_symmetry_space_group_name_H-M C1m1
loop_
_symmetry_equiv_pos_as_xyz
          'x, -y, z'
          'x, y, z'
          'x+1/2, -y+1/2, z'
          'x+1/2, y+1/2, z'
loop_
_atom_site_label
_atom_site_type_symbol
_atom_site_symmetry_multiplicity
_atom_site_fract_x
_atom_site_fract_y
_atom_site_fract_z
_atom_site_occupancy
_atom_site_B_iso_or_equiv
Al al   4 0.25 0.16667 0 1 1
Si si   4 0.0083 0.16667 -0.4444 1 1
O-H1 o   4 -0.0458 0.83333 0.1181 1 1
O-H2 o   2 0.0458 0 -0.1181 1 1
O-H3 o   4 0.0083 0.16667 0.3972 1 1
O-H4 o   4 0 0.33333 -0.1181 1 1
O-H5 o   2 0.5 0 0.1181 1 1
O1 o   2 0.0333 0 0.625 1 1
O2 o   4 0.2833 0.25 0.625 1 1
```